Journal of Biomedical Optics

BiomedicalOptics.SPIEDigitalLibrary.org

Investigation of alterations in multifractality in optical coherence tomographic images of *in vivo* human retina

Nandan Kumar Das
Sabyasachi Mukhopadhyay
Nirmalya Ghosh
Jay Chhablani
Ashutosh Richhariya
Kompalli Divakar Rao
Naba Kishore Sahoo

SPIE.

Nandan Kumar Das, Sabyasachi Mukhopadhyay, Nirmalya Ghosh, Jay Chhablani, Ashutosh Richhariya, Kompalli Divakar Rao, Naba Kishore Sahoo, "Investigation of alterations in multifractality in optical coherence tomographic images of *in vivo* human retina," *J. Biomed. Opt.* **21**(9), 096004 (2016), doi: 10.1117/1.JBO.21.9.096004.

Investigation of alterations in multifractality in optical coherence tomographic images of *in vivo* human retina

Nandan Kumar Das,[a] Sabyasachi Mukhopadhyay,[a,b] Nirmalya Ghosh,[a] Jay Chhablani,[c] Ashutosh Richhariya,[c] Kompalli Divakar Rao,[d,*] and Naba Kishore Sahoo[e]
[a]Indian Institute of Science Education and Research Kolkata, Mohanpur 741 246, India
[b]Nanoscope Technologies Pvt. Ltd., New Town Rajarhat 700156, India
[c]L. V. Prasad Eye Institute, Kallam Anji Reddy Campus, Banjara Hills, Hyderabad 500 034, India
[d]Bhabha Atomic Research Centre Facility, Photonics and Nanotechnology Section, Autonagar, Visakhapatnam 530012, India
[e]Bhabha Atomic Research Centre, Atomic and Molecular Physics Division, Trombay, Mumbai 400085, India

Abstract. Optical coherence tomography (OCT) enables us to monitor alterations in the thickness of the retinal layer as disease progresses in the human retina. However, subtle morphological changes in the retinal layers due to early disease progression often may not lead to detectable alterations in the thickness. OCT images encode depth-dependent backscattered intensity distribution arising due to the depth distributions of the refractive index from tissue microstructures. Here, such depth-resolved refractive index variations of different retinal layers were analyzed using multifractal detrended fluctuation analysis, a special class of multiresolution analysis tools. The analysis extracted and quantified microstructural multifractal information encoded in normal as well as diseased human retinal OCT images acquired *in vivo*. Interestingly, different layers of the retina exhibited different degrees of multifractality in a particular retina, and the individual layers displayed consistent multifractal trends in healthy retinas of different human subjects. In the retinal layers of diabetic macular edema (DME) subjects, the change in multifractality manifested prominently near the boundary of the DME as compared to the normal retinal layers. The demonstrated ability to quantify depth-resolved information on multifractality encoded in OCT images appears promising for the early diagnosis of diseases of the human eye, which may also prove useful for detecting other types of tissue abnormalities from OCT images. [DOI: 10.1117/1.JBO.21.9.096004]

Keywords: optical coherence tomography; fractals; multifractal analysis; retinal layers; diabetic macular edema.

Paper 160193R received Mar. 29, 2016; accepted for publication Aug. 16, 2016; published online Sep. 9, 2016.

1 Introduction

Optical coherence tomography (OCT) is a well-established depth-resolved imaging method in ophthalmology because of its capability to delineate ultrastructural features of retinal layers *in vivo* and other biological tissues in real time.[1,2] OCT maps the backscattered light intensity distribution for three-dimensional imaging in real time.[1,2] Light scattering occurs in biological tissue from weak variation of the local refractive index in submicron- to several micron-length scales.[3–8] Recent advances in the spectral domain and swept source-based OCT systems make this method an important diagnostic tool for retinal disease care such as the treatment of glaucoma.[9–13] Further, the OCT-based imaging study of acute coronary syndromes has evolved as a potential tool for monitoring the heart at the time of surgical interventions.[14] Moreover, it has also shown considerable potential to image the hard and soft tissues of the oral cavity[15] for detection of malignancy and dental diseases. Indeed, *in vivo* endoscopic OCT has yielded promising results for the diagnosis of cancers and precancers of human mucosa.[16] OCT is routinely being used to monitor alterations in the thickness of retinal layers as disease progresses. However, subtle morphological changes in early disease progression may not be reflected in thickness measurements.[17] Development of methods that can extract and quantify subtle morphological changes in the depth distribution of the refractive index associated with early development of DME is therefore of considerable current interest.

It has been shown that the spatial variation of the refractive index in biological tissues exhibits statistical self-similarity. The light scattering from such self-similar structures has been initially modeled under a monofractal (self-similarity exhibiting a single scaling exponent) hypothesis using the Born approximation.[18] The Fractal (self-similar) and multifractal (multiscale self-similarity exhibiting multiple scaling exponents) structures and processes are ubiquitous in nature and have been observed in diverse systems ranging from stock market fluctuations and physiological time series to tissue structures and so forth.[19–23] Multifractality is a special class of self-similarity that can be decomposed into multiple fractal subsets, wherein local scaling exponents (generalized Hurst exponents) quantify the local scaling behavior and a spectrum of scaling exponents is used to completely characterize the multifractality of the signal.[19–23] In contrast to previously employed monofractal approximations, we have recently observed that in cervical tissue, the index fluctuations exhibit multifractality.[22] An inverse analysis model was accordingly developed to quantify the

*Address all correspondence to: Kompalli Divakar Rao, E-mail: divakar@barc.gov.in

1083-3668/2016/$25.00

signature of multifractality from tissue light-scattering signal, which was also initially explored for precancer detection.[23]

Various diseases and disorders of the eye are associated with characteristic morphological changes in different layers of the retina. Analyses of individual layers of the retina are therefore becoming increasingly important with the advent of newer therapeutic approaches. Quantitative studies on the variations of optical densities/indices of different retinal layers through OCT imaging have shown considerable promise for the early detection of central retinal artery occlusion.[24–26] Diabetic macular edema (DME), a retinal disease associated with diabetes, causes the retina to thicken/swell, and the index variation at the edge of the DME in different layers also undergoes characteristic alterations as compared to the healthy layers.[27] There have been only a few studies on the use of quantitative analysis on OCT images. Somfai et al.[28] carried out a monofractal-based analysis of OCT images to quantify retinal tissue damage, followed by Varga et al.,[29] who investigated the differences in texture and optical properties of the retinal tissue in patients with multiple sclerosis. Another recent study employed differentiated box counting-based fractal analysis, and reduction of the fractal dimension in the retinal layers of the diabetic eye compared to healthy retinas was reported.[30] However, considering the complex nature of index variations and the resulting complex spatial correlations, use of a more generalized statistical multiresolution analysis may yield potentially valuable information on multifractality that is otherwise missed by simpler thickness measurements and monofractal analysis of retinal layers. We have therefore employed multifractal detrended fluctuation analysis (MFDFA) on healthy, as well as diseased, retinal OCT images to investigate the diagnostic potential of the derived multifractal properties toward retinal disease detection. To the best of our knowledge, this is the first attempt to use such sophisticated statistical multiresolution analysis on OCT images. MFDFA analysis on normal and diseased human retinal (*in vivo*) OCT images showed interesting and consistent differences in the multifractal properties of the different retinal layers. The results demonstrate the potential of multifractal analysis for the early detection of human eye diseases (such as DME) via the depth-resolved information on multifractality encoded in OCT images. This promising approach may also be extended toward detection of diverse tissue abnormalities from OCT images.

2 Method and Materials

2.1 *Experimental System*

The spectral domain OCT scans of patients were obtained using Cirrus high definition (HD)-OCT 4000 (Carl Zeiss Meditec, Inc., Dublin, California) after dilatation of the pupil with 1% tropicamide and 10% phenylephrine eye drops at the L. V. Prasad Eye Institute, Hyderabad, India. The axial and lateral resolutions of the system are ~5 to 7 μm and ~20 μm, respectively. Cirrus HD-OCT protocols allowed for image averaging to enhance the image contrast and to decrease the speckle noise. The scan protocol used for imaging in this study is an HD 5 line raster scan implying five high-density images, each with 4096 axial scans acquired at 27 KHz. The A-scan probes the depth of 2 mm (in tissue) containing 1024 points. For the diseased cases, one scan out of the five, that had the maximum diameter of the macular hole, was analyzed. The signal strength is graded in 0 to 10 units as an indicator of the signal-to-noise ratio and only scans with a signal strength greater than or equal to 6 were used for analysis. As a control, a spectral domain-OCT scan of a normal retina also was done in healthy subjects. Five different spots from each individual layer of each retinal OCT image have been taken for multifractal analysis. About six different images of the same pathology have been acquired for the analysis. The Institute Review Board (L. V. Prasad Eye Institute) approval was granted for a retrospective study for image analysis from human subjects with informed consent of the patients.

2.2 *Data Analysis*

In the first step, the OCT images from different layers of the healthy retina and near the edge of the DME-affected region of the retina were cropped manually. Following subtraction of the background noise, the resulting images were cropped and unfolded in the vertical direction to generate the one-dimensional (1-D) depth-wise refractive index variations $[\eta(z)]$. Caution was exercised while cropping different layers for Fourier and multifractal analysis. The obtained 1-D index fluctuation series were then subjected to (a) Fourier domain analysis using the sombrero function and (b) MFDFA, a state-of-the-art statistical tool for the quantification of multifractality.

2.2.1 *Fourier domain analysis using the Sombrero function*

Fourier analysis is a simple yet convenient approach to test and quantify self-similar behavior of any stationary fluctuation series via their spatial frequency distribution. To gain some preliminary insight into the nature of the randomness of the index variations of different retinal layers, we have performed Fourier domain analysis using the Sombrero function[31] (constructed from the first-order Bessel function of the first kind) on the unfolded 1-D (depth-wise) index variations.

2.2.2 *Multifractal detrended fluctuation analysis*

The mathematical details of MFDFA can be found elsewhere.[19–23] We have used MFDFA code written in MATLAB® (Mathworks R2010A) software for the multifractal analysis. Briefly, the profile of the unfolded refractive index fluctuation series is first determined as

$$Y(i) = \sum_{k=1}^{i} [x_k - \langle x \rangle], \quad \text{where } i = 1, 2, \ldots, N. \tag{1}$$

The resulting profile $Y(i)$ is divided into $N_s = \text{int}\,(N/s)$ nonoverlapping segments ν of equal length s. The local trend of the series $[y_\nu(i)]$ is then determined by least-square polynomial fitting of the series, and the resulting variance is determined

$$F^2(\nu, s) = \frac{1}{s} \sum_{i=1}^{s} \{Y[(\nu - 1)s + i] - y_\nu(i)\}^2. \tag{2}$$

The moment (q)-dependent fluctuation function is then extracted by averaging over all the segments as

$$F_q(s) = \left\{ \frac{1}{2N_s} \sum_{\nu=1}^{2N_s} [F^2(\nu, s)]^{\frac{q}{2}} \right\}^{1/q}. \tag{3}$$

The scaling behavior is then quantified by analyzing the variations of $F_q(s)$ versus s for each value of q. For this purpose, the general scaling function is assumed to follow a power law behavior

$$F_q(s) \sim s^{h(q)}. \tag{4}$$

The number of segments, $N_s = \text{int}(N/s)$, depends on the length of the unfolded data series ($N \sim 2000$) and scale length (s) for which the fluctuation function $[F_q(s)]$ has to be calculated. The segment numbers, N_s should be sufficiently large to have a statistically reliable in averaging procedure in Eq. (3). On the other hand, systematic deviation of scaling behavior from Eq. (4) may occur for very small N_s. This was handled by limiting the range of length scale $s \sim 8$ to 29 in our study. Note that the scale number s can be replaced by a length scale, $l = s \times$ resolution of retinal OCT ($\sim 5\ \mu$m). Then, Eq. (4) can be written as

$$F_q(l) \sim l^{h(q)}. \tag{5}$$

The multifractal signal is subsequently characterized via the generalized Hurst scaling exponent $h(q)$, the classical multifractal scaling exponent $\tau(q)$, and the singularity spectrum $f(\alpha)$. These are related as[19]

$$\tau(q) = qh(q) - 1, \tag{6}$$

$$\alpha = \frac{d\tau}{dq}, \quad f(\alpha) = q\alpha - \tau(q), \tag{7}$$

where α is the singularity strength or the Holder exponent and the width $\Delta\alpha$ defined at the minimum value of $f(\alpha)$ is a quantitative measure of multifractality.

We note in passing that for a stationary monofractal series, $h(q = 2)$ is equivalent to the Hurst scaling exponent H.[19] Here, values for the Hurst exponent ($H = 0.5$, >0.5, and <0.5) correspond to uncorrelated random (Brownian) fluctuations, long-range correlations or persistent behavior, and short-range correlations or antipersistent behavior, respectively.[19,22,23]

3 Results and Discussion

The *in vivo* retinal OCT image of a representative healthy retina is shown in Fig. 1(a) and the corresponding OCT image of a patient with DME is shown in Fig. 1(b). Figure 1(c) displays a typical depth (z) variation of the refractive index $\eta(z)$ for different retinal layers corresponding to the red line in Fig. 1(a). Figure 1(d) generated from Fig. 1(b) displays representative refractive index fluctuation close to the edge of the DME (green line) and far from the DME (red line) to highlight the visual differences of depth-wise refractive index fluctuations of the OPL layer. However, for analytical purposes, we have cropped images from different layers of healthy retinas and unfolded them to have a sufficiently long data series for MFDFA [displayed in Fig. 3(a)]. In the case of DME-affected retinas, we have cropped the image from different layers in the closed region to the edge of the DME and unfolded them to have a sufficiently long data series for further analysis. The different layers of the retina are: inner limiting membrane (ILM), nerve fiber layer (NFL), ganglion cell layer (GCL), inner plexiform layer (IPL), inner nuclear layer (INL), outer plexiform layer (OPL), outer nuclear layer (ONL), external limiting membrane (ELM), junction of inner and outer photoreceptor segments (IS/OS), outer segment photoreceptor/RPE complex (OPR), retinal

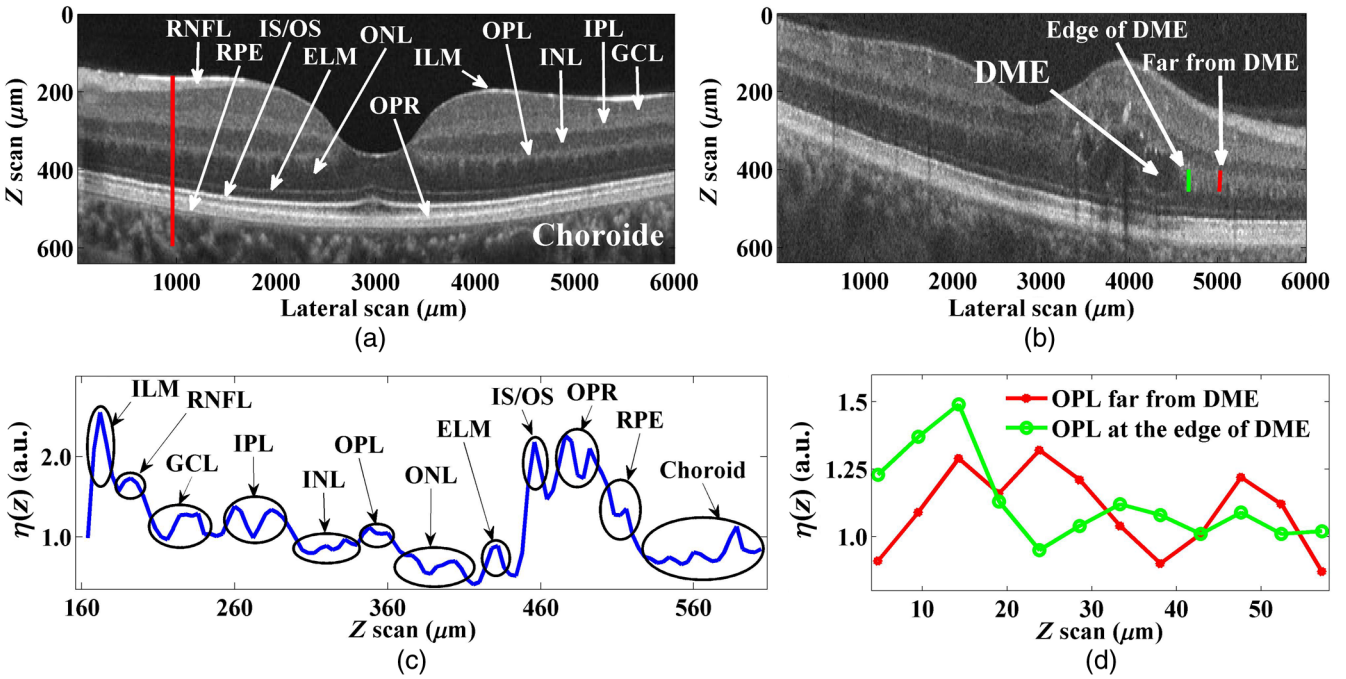

Fig. 1 (a) *In vivo* retinal OCT image of a representative healthy retina. The displayed distinguishable individual layers are segmented manually. The red line indicates the selected region, which is subsequently shown in Fig. 1(c) as depth-wise index variation. (b) Retinal OCT image of a patient with DME disease. The regions of the OPL, near the edge of DME (green line) and far away from DME (red line) are marked. (c) The depth-wise 1-D index variation for the healthy retina [corresponding to red line in Fig. 1(a)]. Different layers are marked using elliptical enclosures. (d) The depth-wise 1-D index variation for the patient with DME for the marked regions [green circle: near the edge of DME and red pentagon: away from DME in OPL corresponding to Fig. 1(b)].

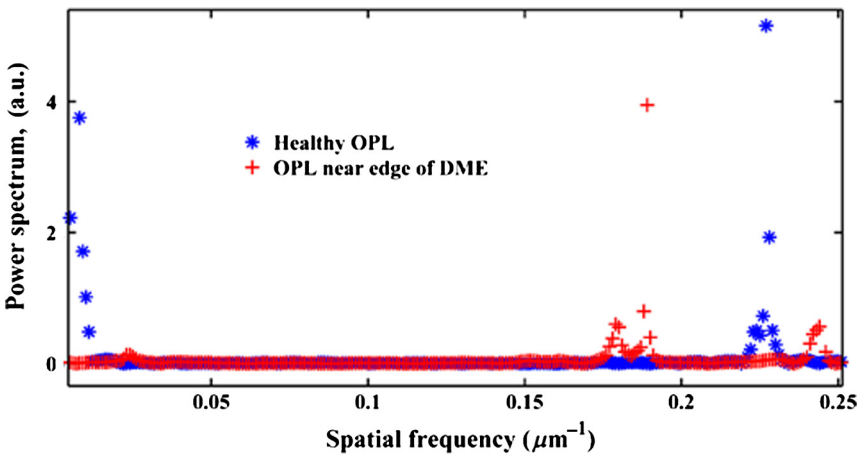

Fig. 2 Fourier domain analysis using sombrero function on the unfolded 1-D (depth-wise) index variations of healthy (shown by blue star) and diseased (DME, red plus) retinal OPL. Considerably increased scatter in the magnitudes at higher spatial frequency regions for the DME-affected OPL layer implies stronger randomness associated with small-scale index variations.

pigment epithelium (RPE), and choroid. Even though there are visual differences in the different layers between the diseased and normal retinas, the underlying depth distributions of index variations leading to the differences need proper quantification. These were therefore analyzed via Fourier domain analysis and multifractal analysis.

Fourier domain analysis enabled extraction of the spatial frequency spectra corresponding to the index inhomogeneity distributions of different retinal layers.[31] An illustrative example of such a Fourier domain analysis is displayed in Fig. 2. The derived spatial frequency spectra between the healthy and diseased (DME) retinal OPL show interesting differences. Specifically, considerably more scatter in the magnitudes at higher spatial frequency regions for the DME-affected OPL layer indicates a higher degree of randomness in the small-scale index fluctuations. The observed two peaks and their widths in the spatial frequency distribution for the DME-affected layer (as opposed to a single peak in a healthy retina) is a manifestation of this randomness compared to a healthy retina. To obtain further quantitative information on the

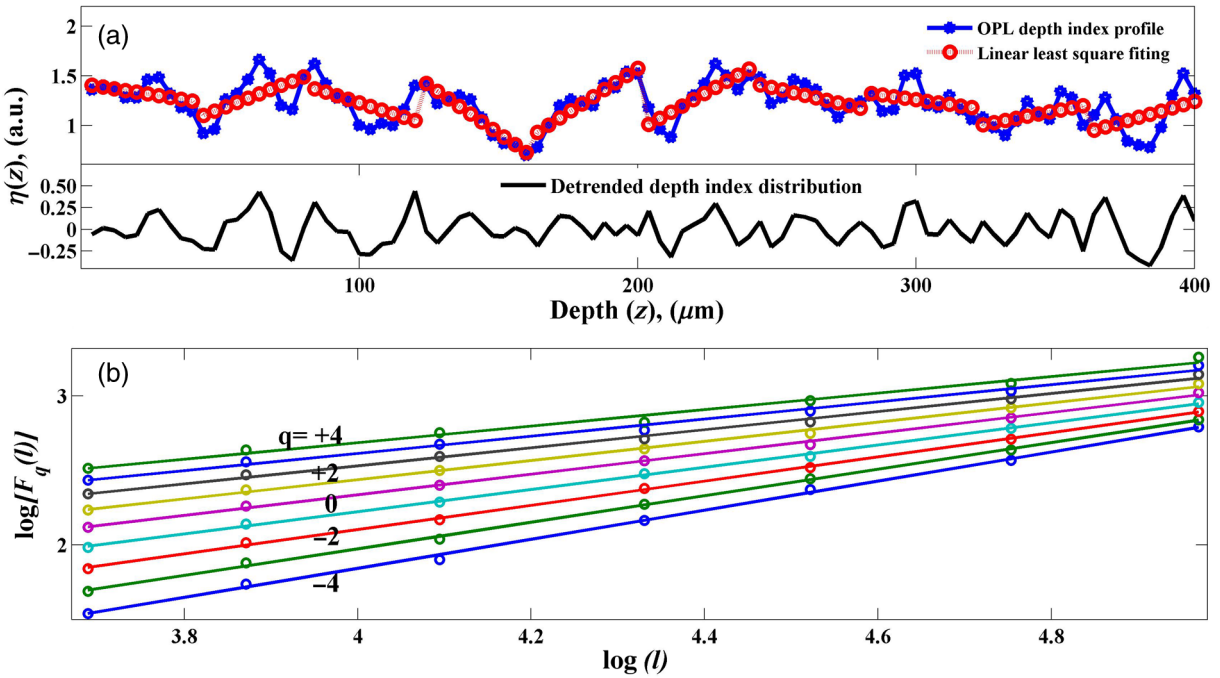

Fig. 3 Various steps of MFDFA analysis on the unfolded 1-D index variations. (a) Upper panel shows unfolded index variation (blue pentagon) for the OPL from healthy retina [corresponding to Fig. 1(a)] and the local linear (first-order polynomial) fit [$y_\nu(i)$ of Eq. (1)] (red circle) for a particular segment corresponding to a typical window size $s = 8$, and lower panel displays corresponding detrended depth index profile (black line, for $s = 8$, depth ~400 μm). (b) The log–log plot of the moment ($q = -4$ to $+4$, shown here)-dependent fluctuation function $F_q(l)$ versus l [derived using Eq. (5)] corresponding to the detrended fluctuations of the OPL from five different spots on a healthy retina.

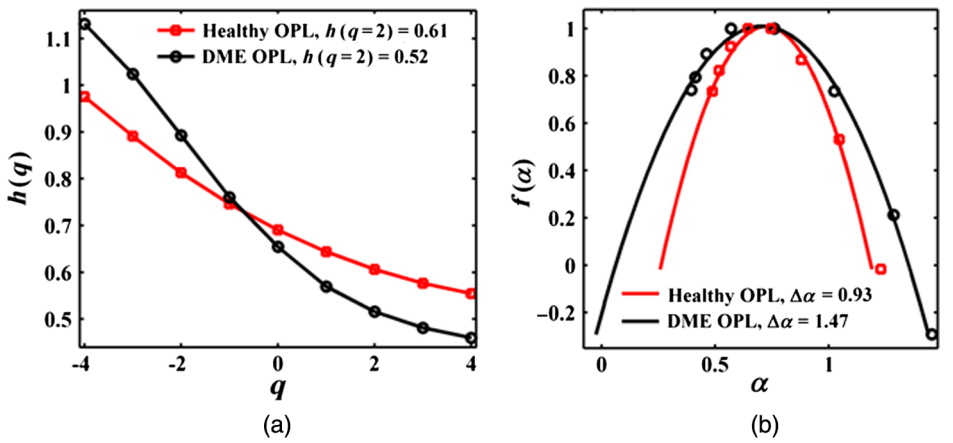

Fig. 4 Comparison of the MFDFA-derived multifractal parameters from typical healthy and diseased (DME) retinal OPLs. (a) Moment dependence of generalized Hurst exponent $h(q)$ (shown for $q = -4$ to 4) for healthy retinal OPL (square symbol, red line) and DME-affected diseased retinal OPL (circle, black line). The values for $h(q = 2)$ are noted. (b) The derived singularity spectrum $f(\alpha)$ for healthy (square, red line) and DME-affected (circle, black line) retinal OPLs. In (a) and (b), the symbols represent data and the lines are guides for the eye. Values for the width $\Delta\alpha$ defined at a minimum value of $f(\alpha)$ are noted.

multifractal nature of the randomness of the index variations, these unfolded depth-index fluctuations were subjected to MFDFA analysis.

Figure 3 displays various steps of the MFDFA analysis on the unfolded 1-D index variations. The presence of various large- and small-scale index variations is apparent in the detrended index fluctuation series [lower panel of Fig. 3(a)] for OPL from healthy retinas. Importantly, the resulting slope of the log–log plot of the constructed fluctuation function $F_q(l)$ versus l [Fig. 3(b)] is observed to vary significantly with varying moment q, implying the presence of strong multifractality. Note that the proposed MFDFA method captured self-similarity over a particular length scale range ($l \sim 40$ to 145 μm) in our present study and this analysis accounted for minimum-length scale equal to the OCT resolution (~5 μm), which was otherwise hidden in the simple thickness measurement. The strength of multifractality was subsequently quantified via the moment-dependent generalized Hurst exponent [$h(q)$] [using Eq. (5)] and the width [$\Delta\alpha$ defined at minimum value of $f(\alpha)$] of the singularity spectrum $f(\alpha)$ [using Eq. (7)]. The analysis was performed on the unfolded 1-D index fluctuation series (obtained via appropriate cropping and subsequent depth-wise unfolding) from different layers at the region close to the edge of retinal DME and from healthy retinal layers. Although the analysis was performed separately on different layers, we pay particular attention to the OPL layer, since it appears to be the most affected by the DME disease. Figure 4 shows a comparison of the MFDFA-derived generalized Hurst exponent [$h(q)$] and the singularity spectrum $f(\alpha)$ of five spots on typical healthy and diseased (DME) OPLs. As expected, strong multifractality is manifested as significant variations of $h(q)$ [Fig. 4(a)] and the resulting considerable width of the singularity spectrum $f(\alpha)$ [Fig. 4(b)] for both healthy and diseased OPLs. The observed differences can be summarized as: (a) the value for $h(q = 2)$ is reduced from 0.61 to 0.52 for affected OPLs (at the area close to the edge of the DME) as compared to healthy OPLs and (b) the strength of multifractality quantified via the width of the singularity spectrum ($\Delta\alpha$) increased from $\Delta\alpha = 0.93$ to 1.47 for the healthy to the DME-affected OPLs, respectively. A decrease of the parameter $h(q = 2)$ is indicative of stronger randomness (or less correlated index variations), possibly originating from increased roughness/heterogeneity of the medium (predominance of index inhomogeneities having smaller spatial dimensions). The increased heterogeneity in index fluctuations is also manifested as stronger multifractality (increased magnitude of $\Delta\alpha$) in the DME-affected OPL. Note that even though the Fourier analysis (sombrero function) also predicted increased randomness of index variations in DME-affected OPLs (Fig. 2 and subsequent discussion), derivation and quantification of the otherwise hidden information on the multifractal nature of the (depth-wise) index variations are exclusively enabled by the MFDFA analysis.

While the results presented in Fig. 4 corresponded to OPL layers of a healthy and a DME-affected retina, the MFDFA analysis was also performed separately on different layers of healthy retinas and diseased retinas with age-related macular

Table 1 Summary of MFDFA analysis on the 1-D (depth-resolved) index variations (obtained from OCT images) from healthy and AMD-affected retinas. The mean values (along with standard deviations) for the generalized Hurst exponent $h(q = 2)$ and the width of the singularity spectrum $\Delta\alpha$ for five healthy and five diseased retinas with five different spots on each individual image layer are summarized. The results are shown separately for different retinal layers.

Retinal layers	$h(q = 2)$		$\Delta\alpha$	
	Healthy	AMD-affected	Healthy	AMD-affected
NFL	0.87 ± 0.04	0.66 ± 0.01	0.62 ± 0.08	0.93 ± 0.09
GCL	0.81 ± 0.03	0.61 ± 0.02	0.85 ± 0.02	1.57 ± 0.07
IPL	0.72 ± 0.02	0.66 ± 0.03	0.77 ± 0.05	1.23 ± 0.08
OPL	0.62 ± 0.01	0.53 ± 0.02	0.97 ± 0.09	1.46 ± 0.10
ONL	0.61 ± 0.03	0.51 ± 0.02	1.02 ± 0.07	1.31 ± 0.06
Choroid	0.76 ± 0.04	0.57 ± 0.03	0.82 ± 0.08	1.27 ± 0.12

degeneration (AMD). The results of this analysis carried out on five healthy and five AMD retinal images with five different spots of each individual image layer are summarized in Table 1. Although the estimated values for the parameters, the generalized Hurst exponent $[h(q)]$, and the width of the singularity spectrum $(\Delta\alpha)$ varied from layer to layer and sample to sample, the results showed a consistent trend in that the diseased or abnormal retinas were always associated with a decreased value of $h(q=2)$ and increased magnitude of $\Delta\alpha$. These results clearly demonstrate that diseased retinal layers are associated with increased randomness and heterogeneity in depth-wise index variations, information on which can be extracted and quantified via MFDFA analysis.

4 Conclusions

To summarize, multiresolution analysis revealed a clear signature of multifractality in depth-wise index variations of different retinal layers, as encoded in *in vivo* OCT images. The index variations in a given layer of the diseased retina were found to be more random (less correlated) compared to those of healthy retinal layers, manifested as a decrease in the generalized Hurst exponent. Moreover, the strength of multifractality was also significantly higher in diseased retinal layers. The demonstrated ability to quantify the nature of the randomness and the hidden multifractal information on the depth distribution of tissue refractive indices by employing MFDFA on *in vivo* OCT images should prove valuable for the diagnosis of diseases of the human eye. In general, the use of such multifractal analysis on OCT images may lead to a diagnostic modality for the detection of various other types of tissue abnormalities, exploring tissue multifractality as a potential biomarker.

Acknowledgement

NKD, SM, and NG would like to thank BRNS-DAE, CSIR, IISER Kolkata, MHRD, Government of India for funding and facilities.

References

1. J. A. Izatt and M. A. Choma, *Optical Coherence Tomography: Technology and Applications*, W. Drexler and J. G. Fujimoto, Eds., Chap. 2, Springer-Verlag, Berlin, Heidelberg (2008).
2. J. G. Fujimoto et al., "Optical coherence tomography: an emerging technology for biomedical imaging and optical biopsy," *Neoplasia* **2**(1–2), 9–25 (2000).
3. L. Cherkezyan et al., "Interferometric spectroscopy of scattered light can quantify the statistics of subdiffractional refractive-index fluctuations," *Phys. Rev. Lett.* **111**, 033903 (2013).
4. W. Choi et al., "Tomographic phase microscopy," *Nat. Methods* **4**, 717–719 (2007).
5. A. Wax and V. Backman, *Biomedical Applications of Light Scattering*, McGraw Hill Publishing, New York City (2009).
6. J. M. Schmitt and G. Kumar, "Turbulent nature of refractive-index variations in biological tissue," *Opt. Lett.* **21**, 1310–1312 (1996).
7. N. N. Boustany, S. A. Boppart, and V. Backman, "Microscopic imaging and spectroscopy with scattered light," *Annu. Rev. Biomed. Eng.* **12**, 285–314 (2010).
8. M. Born and E. Wolf, *Principles of Optics*, Cambridge University Press, Cambridge, England (1999).
9. B. E. Bouma et al., "Fourier-domain optical coherence tomography: recent advances toward clinical utility," *Curr. Opin. Biotechnol.* **20**(1), 111–118 (2009).
10. E. Garcia-Martin et al., "Intra and interoperator reproducibility of retinal nerve fibre and macular thickness measurements using Cirrus Fourier domain OCT," *Acta Ophthalmol.* **89**(1), e23–e29 (2011).
11. M. Wojtkowski et al., "In vivo human retinal imaging by Fourier domain optical coherence tomography," *J. Biomed. Opt.* **7**(3), 457–463 (2002).
12. B. Potsaid et al., "Ultrahigh speed spectral/Fourier domain OCT ophthalmic imaging at 70,000 to 312,500 axial scans per second," *Opt. Express* **16**(19), 15149–15169 (2008).
13. H. Li et al., "Anterior segment optical coherence tomography and its clinical applications in glaucoma," *J. Curr. Glaucoma Pract.* **6**(2), 68–74 (2012).
14. F. Prati et al., "OCT-based diagnosis and management of stemi associated with intact fibrous cap," *JACC Cardiovasc. Imaging* **6**(3), 283–287 (2013).
15. B. W. Colston et al., "Imaging of hard- and soft-tissue structure in the oral cavity by optical coherence tomography," *Appl. Opt.* **37**(16), 3582–3585 (1998).
16. A. M. Sergeev et al., "In vivo endoscopic OCT imaging of precancer and cancer states of human mucosa," *Opt. Express* **1**, 432–440 (1997).
17. W. Gao et al., "Investigation of changes in thickness and reflectivity from layered retinal structures of healthy and diabetic eyes with optical coherence tomography," *J. Biomed. Sci. Eng.* **4**, 657–665 (2011).
18. M. Hunter et al., "Tissue self-affinity and polarized light scattering in the born approximation: a new model for precancer detection," *Phys. Rev. Lett.* **97**, 138102 (2006).
19. J. W. Kantelhardt et al., "Multifractal detrended fluctuation analysis of non-stationary time series," *Physica A* **316**, 87–114 (2002).
20. P. C. Ivanov et al., "Multifractality in human heartbeat dynamics," *Nature* **399**, 461–465 (1999).
21. L. A. N. Amaral et al., "Behavioral-independent features of complex heartbeat dynamics," *Phys. Rev. Lett.* **86**, 6026–6029 (2001).
22. N. Das et al., "Probing multifractality in tissue refractive index: prospects for precancer detection," *Opt. Lett.* **38**, 211–213 (2013).
23. N. Das et al., "Tissue multifractality and Born approximation in analysis of light scattering: a novel approach for precancers detection," *Sci. Rep.* **4**, 6129 (2014).
24. D. Barthelmes et al., "Differential optical densities of intraretinal spaces," *Invest. Ophthalmol. Visual Sci.* **49**(8), 3529–3534 (2008).
25. M. Neudorfer et al., "Differential optical density of subretinal spaces," *Invest. Ophthalmol. Visual Sci.* **53**(6), 3104–3110 (2012).
26. H. Chen et al., "Quantitative analysis of retinal layers' optical intensities on 3D optical coherence tomography for central retinal artery occlusion," *Sci. Rep.* **5**, 9269 (2015).
27. T. A. Ciulla, A. G. Amador, and B. Zinman, "Diabetic retinopathy and diabetic macular edema," *Diabetes Care* **26**, 2653–2664 (2003).
28. G. M. Somfai et al., "Fractal-based analysis of optical coherence tomography data to quantify retinal tissue damage," *BMC Bioinf.* **15**, 295 (2014).
29. B. E. Varga et al., "Investigating tissue optical properties and texture descriptors of the retina in patients with multiple sclerosis," *PLoS One* **10**(11), e0143711 (2015).
30. W. Gao et al., "Investigation of changes in fractal dimension from layered retinal structures of healthy and diabetic eyes with optical coherence tomography," *Proc. SPIE* **9541**, 95411I (2015).
31. J. Goodman, *Introduction to Fourier Optics*, 3rd ed., Roberts and Company Publishers, Englewood (2004).

Biographies for all the authors are not available.